Vapor Condensation in the Mixing Zone of a Jet

GEORGE M. HIDY and S. K. FRIEDLANDER

The Johns Hopkins University, Baltimore, Maryland

Experimental studies were made of fog formation in free jets containing glycerine and dibutyl phthalate. Visual and photographic observations showed that condensation took place near the nozzle in the mixing zone between the jet and the ambient air. Fog formation began at a well-defined location downstream from the nozzle depending on the initial velocity, temperature, and concentration of vapor. The location could be changed by inserting solid bodies or by adding foreign nuclei to the mixing zone. Measurements were made of mean temperature and concentration profiles in the mixing zone with noncondensable gases. These compared well with the predictions of turbulent boundary-layer theory. Calculations were made of the supersaturation to be expected in the case of glycerine. Downstream of the point where condensation first occurred fog filled most of the region where the calculated supersaturation was above unity. Based on the experimental evidence a mechanism is proposed for condensation in a free jet.

Saturation or supersaturation may be produced in vapor-air mixtures as a result of a number of physical processes including surface cooling, adiabatic or nearly adiabatic expansion, radiative heat loss, and mixing of the hot vapor with cool air. It is with the last process that this paper is concerned.

Anyone exhaling on a cool day has witnessed fog formation by this mechanism. The condensation trail (contrail) which forms during dilution and cooling of hot, moist, exhaust gases from aircraft engines is another example (3). Jet mixing is used to produce screening smokes for military applications as well as agricultural aerosols for pest control (9). Mixing also contributes to the formation of fogs and other atmospheric aerosols. It has been proposed that jet mixing be used to test the Becker-Döring theory of condensation (12).

The system chosen for experimental study was a hot jet of a condensable vapor-air mixture which mixed with air at room temperature. The system has practical interest, and a considerable body of information on fluid mechanics and heat transfer in the turbulent jet is available. Some of this is reviewed by Hinze (14) and Townsend (27).

Studies of condensation in a turbulent jet have been made by Amelin (1) and co-workers (2), Higuchi and O'Konski (12), and Levine and Friedlander (16). Amelin and Higuchi and O'Konski used jet mixing to test the predictions of the Becker-Döring theory of nucleation. Levine and Friedlander observed the limits of jet temperature and concentration necessary for detectable fog formation. In none of these studies were detailed observations made of the zone of fog formation or of the concentration and temperature distributions in the condensing jet. Such measurements are reported in this study. The emphasis is on the application of continuum theories of the transport phenomena to the condensation process. A mechanism is offered for the method by which fog formation takes place.

A complete solution of the condensation problem in a turbulent mixing system would require a solution of the equations of conservation of mass, energy, and momentum, including an expression for the kinetics of condensation. Such a solution does not exist. Friedlander (7) has proposed a method for dimensionally modeling a system in which condensation is produced by mixing. As one of the important dimensionless parameters he introduced the Damköhler group for condensation $L/V\,\tau_C$.

Levine and Friedlander (16) noted that in the case of the free jet the equations of conservation of species and energy are identical in form up to the region of condensation when the Lewis number is equal to 1. In this case the dimensionless concentrations and temperatures should be equal:

$$\frac{y_A - y_{A\infty}}{y_{A_0} - y_{A\infty}} = \frac{T - T_\infty}{T_0 - T_\infty} \qquad (1)$$

It is easy to see that in the turbulent system the same result will hold in terms of the local average concentration (mole fraction) $\overline{y_A}$ and temperature $\overline{T}$ when the turbulent Lewis number is unity and the molecular diffusivities can be neglected in comparison with the eddy diffusivities. From the relationship between the concentration and temperature fields it is possible to place limits on the concentrations and temperatures which must exist at the jet orifice for condensation to occur. However the method gives no information about the magnitude of the supersaturation which can exist in the system or of the detailed structure of the condensation zone. Such information is presented in this study.

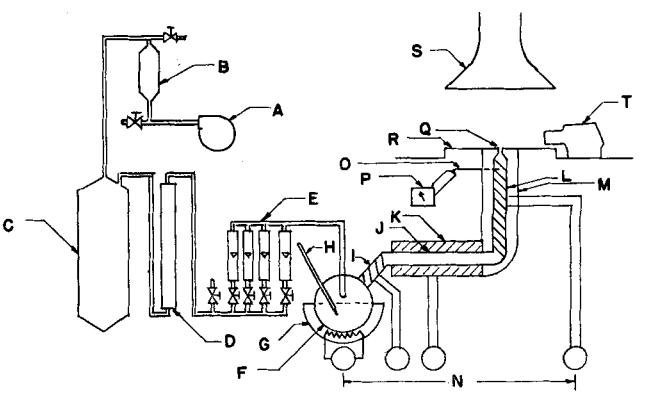

Fig. 1. The aerosol generator.

George M. Hidy is with the National Center for Atmospheric Research, Boulder, Colorado.

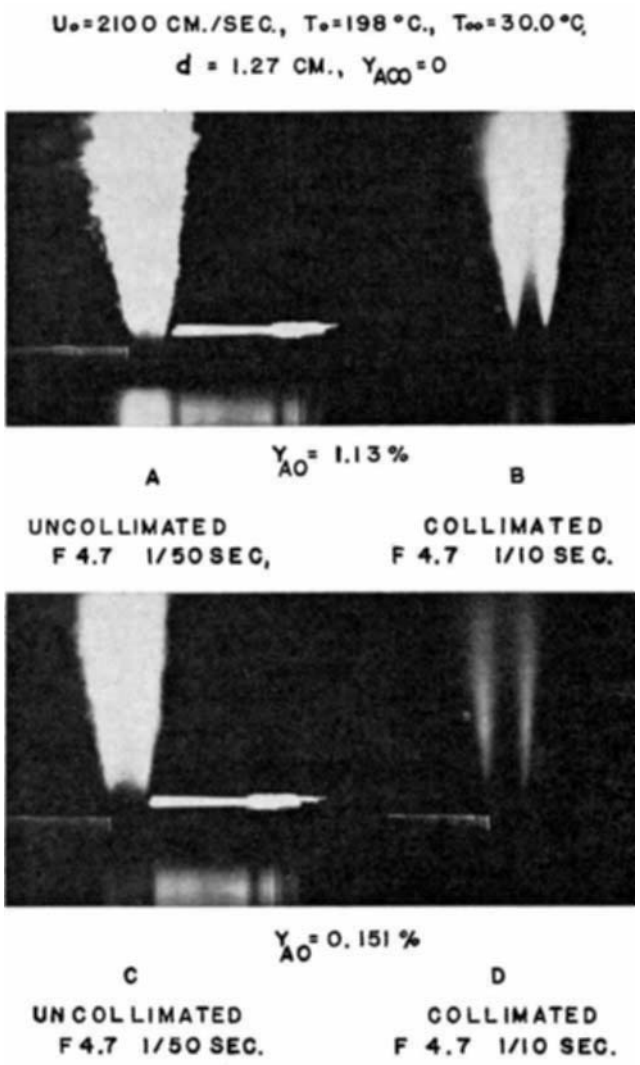

Fig. 2. Glycerine fog formation in jet flow.

EXPERIMENTAL METHOD

The Aerosol Generator

The basic equipment consisted of an aerosol generator similar to the design of Levine and Friedlander (*16*). This is essentially a device for producing air-condensable vapor mixtures at known concentrations, temperatures, and flow rates. Figure 1 shows a schematic diagram of the important features of the unit.

A rotary compressor (A) supplied air to the generator. The air was pumped through an oil trap (B), a surge tank (C), and a dust and oil filter (D) packed with glass wool. From the filter, air passed through a calibrated metering system (E) consisting of four rotameters. The volumetric flow was adjusted and measured before entering the vaporizer (F). Air flowed into the vaporizer through a nozzle designed to direct the air across the surface of the liquid. A heater (G) covering the vaporizer regulated the temperature of the aerosol liquid which controlled the average vapor concentration. The liquid temperature in the vaporizer was measured with a thermometer (H). The gas-vapor mixture flowed through a connecting system (I) heated by an insulated coil into a 15 in. long, 1-in. diameter vycor glass mixing section packed with either stainless steel screen or Pyrex glass raschig rings (J). A regulated furnace (K) heated the packed tube. Flow continued into a 14 in. long, 1-in. diameter stainless steel approach section (L) which was heated by two ½-in. heating tapes covered with asbestos pipe insulation (M). The bank of powerstats (N) was used to regulate the heaters. The temperature in the approach section was measured with an iron-constantan thermocouple probe (O). A potentiometer (P) recorded the thermocouple responses.

The nozzle (Q) was designed with a reduction from the 1-in. in diameter approach to either a ½- or ¼-in. orifice over an axial distance of ⅞ in. To produce flat profiles of the velocity, temperature, and concentration 18-mesh screens were placed 2 and 14 in. below the orifice. The nozzle fitted into an 11- by 18-in. transite floor (R). The fog was removed from the laboratory by a bell shaped exhaust hood (S) which measured 18 in. in diameter at the lower edge. The lower edge of the hood was placed 14 in. above the transite floor.

The air in the laboratory was not dried. Humidity during most of the experiments was monitored by a recording psychrometer. The relative humidity in the laboratory varied from 35 to 76%, but fog formation was not visibly affected.

Generation of Hot Vapor-Air Mixtures

The liquids from which aerosols were generated included glycerine and dibutyl phthalate. Diffusion coefficients and related quantities for mixtures of the vapors of these liquids with air are given in Table 1. Most of the results reported in this paper concern the glycerine aerosol.

To generate the superheated vapor a known weight of liquid was placed in the vaporizer and heated to the desired temperature. Simultaneously the mixing and nozzle sections were heated to prevent condensation on the walls of the apparatus. After the desired temperature was reached, the compressor was started and the air flow was adjusted to operating conditions. Flow rates and vaporizer temperatures were maintained constant (flow ± 1 to 2% and T ± 2.0°C. maximum deviation). The nozzle temperature was adjusted during a run by regulating the heaters surrounding the piping. This temperature was kept at a constant value (± 2°C.) for at least ½ hr. before measurements were made. The average vapor concentration at the nozzle was determined by the weight loss of liquid in the vaporizer and the air flow rate. No significant loss of material occurred before the compressor was started. The generator came to a steady state within 30 min. After approximately 90 to 120 min. total running time observations and experimental measurements were begun.

Some thermal decomposition eventually occurred in all the liquids. Therefore fresh material was used after approximately 12 to 20 hr. running time.

Illumination and Photographic Equipment

Visual and photographic observations were made with a 300-w. slide projector as a light source. The projector was placed on the side of the transite floor at right angles to the point of observation [Figure 1 (T)]. The fog cloud was viewed against a black background with light from this source with and without collimation.

The photographs were taken with a Graflex Crown Graphic camera and Eastman Kodak Royal Pan film. Conditions for photography generally included an f-stop of f/4.7 and a shutter speed of 1/5 to 1/50 of a second. The camera was placed 18 to 20 in. from the nozzle edge at right angles to the illumination source.

Velocity, Temperature, and Concentration Measurements

Detailed measurements were made of the distributions of concentration, temperature, and velocity in the mixing zone of the jet. Additional measurements were made in the transition and fully developed regions. In all cases the measurements were made with the 1.27 cm. nozzle operated at U_o = 2,100

Table 1. Transport Properties of Gases and Vapors in Air

Component A	T(°K.)	D_A (sq. cm./sec.)	Ref.	N_{Pr}*	N_{Sc}	N_{Le}
Glycerine	398	0.111	*17*	0.70	2.3	0.30
Dibutyl phthalate	408	0.064	*15*	0.69	4.1	0.17
Helium	298	0.713†	—	0.72	0.22	3.3
Carbon dioxide	273	0.138	29	0.72	0.96	0.75
Freon-114	298	0.0805†	—	0.72	2.0	0.36

* McAdams (*18*), pp. 483.
† Calculated by the method of Hirschfelder, et al. [Reid and Sherwood (*22*), pp. 268 ff.].

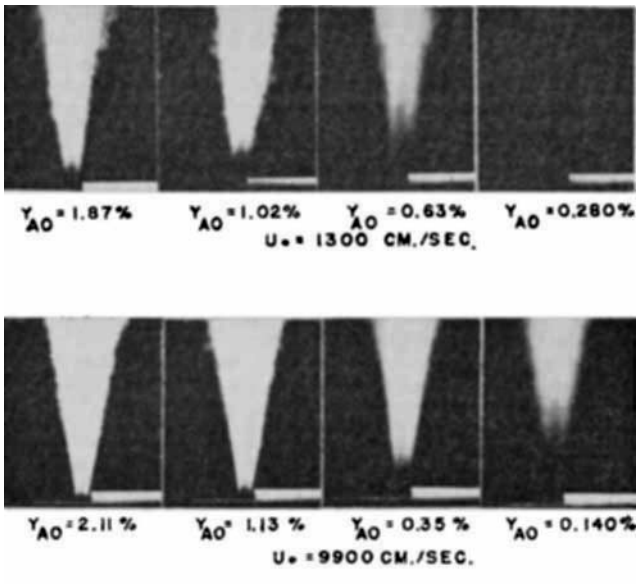

Fig. 3. Glycerine fog formation, effect of varying U_o and y_{Ao} (T_o = 198°C.).

cm./sec. and T_o = 198°C. The velocity distribution was determined with an impact tube, and temperature profiles were obtained with an iron-constantan thermocouple probe. No measurements were made of the concentration distributions of the condensable vapors in the jet. Instead small amounts of helium, carbon dioxide, and freon-114 were added in separate experiments to the air flow entering the vaporizer, empty of liquid aerosol material. Some of the transport properties of the gas mixtures are listed in Table 1. The gas in the jet was sampled isokinetically by adjusting the sampling velocity of the probe to match the x component of the jet velocity at the sampling point. Average local concentrations were determined with a calibrated thermal conductivity cell.

RESULTS AND DISCUSSION

Observations of Fog Formation in the Jet

Shape of the Condensation Zone. When an uncollimated light beam was shown on the jet at right angles to the observer, the fog appeared as shown in Figure 2A. Collimated light (2-mm. slit width) passing through the center line of the jet revealed the internal structure of the cloud (Figure 2B). The cross section of the fog filled region was roughly that of a wedge with its tip located vertically downstream from the edge of the nozzle. The region where condensation first appeared falls within the turbulent mixing zone between the emerging jet and the ambient air.

To explore the effect of the initial conditions on the wedge of fog the velocity and concentration of vapor at the nozzle were varied with the ¼-in. diameter jet used. The photographs in Figure 3 show that the shape and the optical density of the aerosol cloud depended on both U_o and y_{Ao}. The optical density of the cloud decreased with decreasing concentration, while the distance from the nozzle edge to the tip of the cloud ($\bar{h}$) increased to the point of blow off where the fog was no longer visible. As the initial velocity increased, the distance $\bar{h}$ decreased. Changing the velocity affected the appearance of the cloud less than changing the concentration. The formation of the cloud also depended on the initial temperature. As shown in Figure 4 the fog tended to blow off the nozzle, and the optical density decreased with increase in initial temperature. The same type of behavior was observed with other condensable vapors.

Effect of Inserting Wires and Screens. Wires ranging in diameter from 0.00015 to 0.03 in. were inserted at various points in the jet. When wires of diameter greater than 0.0005 in. were placed in the mixing zone below the cloud, the location of the lower tip of the cloud moved nearer to the edge of the nozzle and appeared to cling to the wire. In some cases the distance $\bar{h}$ could be reduced to 1 to 2 mm. Inserting wires of diameter less than 0.0005 in. had no effect on the point where fog began to form.

Figure 5 shows the effect of inserting an 0.03-in. diameter wire in the jet. When the wire was placed at the center below the cloud, no change was observed in the wedge of fog (Figure 5A). Insertion of the wire in the mixing zone distinctly changed the location of fog formation as shown in Figure 5B. Blunt bodies and vertically oriented flat plates also affected fog formation when placed in the mixing zone, but not when placed in the central core. Fog appeared in the boundary layers formed by the flow around the bodies.

Introduction of an 18-mesh screen below the condensation region produced a striking effect as shown in Figure

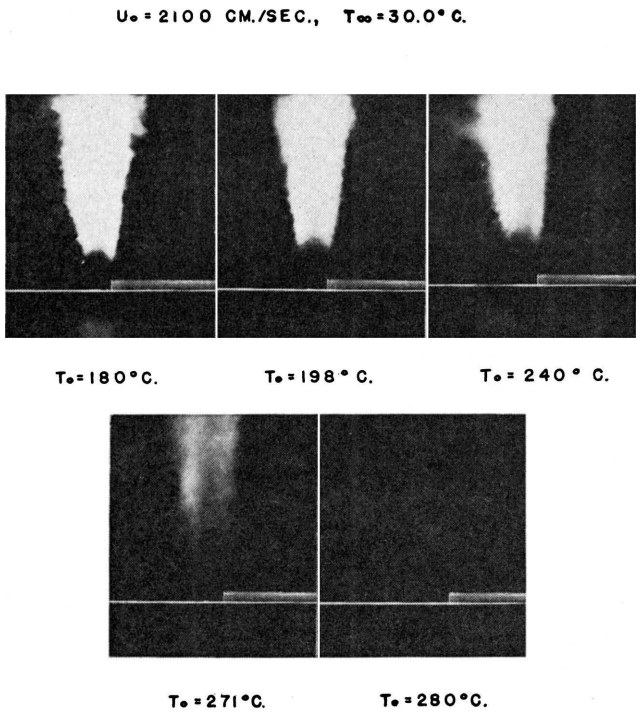

Fig. 4. Glycerine fog formation in jets, effect of initial temperature variation.

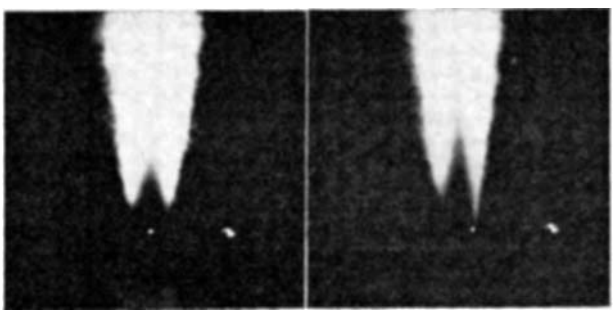

Fig. 5. Glycerine fog formation in a jet, effect of inserting small wires.

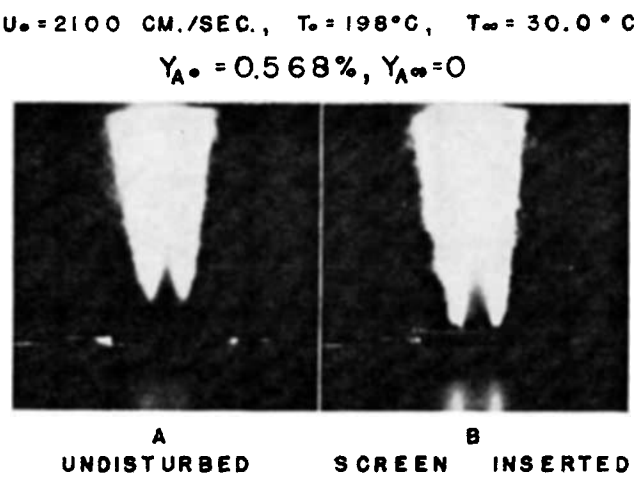

Fig. 6. Glycerine fog formation in jets, effect of inserting wire screens.

6. Photo A represents the undisturbed cloud. Photo B shows that fog formation occurs on the part of the screen that lies in the mixing zone. Heating the screen reversed the effect and tended to decrease the optical density of the cloud.

These experiments indicate (but do not prove) that a supersaturated region exists between the edge of the nozzle and the tip of the wedge of fog. Inserting solid bodies probably produced condensation in the supersaturated region in one of the following ways: the fluid hold up in the boundary layer around the bodies increased the growth time of nuclei, the bodies acted as heat sinks which increased the local supersaturation, the bodies disturbed the flow sufficiently to entrain cool air into the mixing zone, or the bodies acted as nucleation centers for catalyzing the condensation process. The failure of the small wires to disturb the fog is consistent with the four mechanisms. The heat sink mechanism is consistent with the change produced in the cloud when the screen was heated.

Effect of Adding Nuclei. When chalk dust was blown into the jet, the zone of fog formation moved toward the nozzle. In a separate experiment sulfuric acid vapor was introduced by placing droplets of 96% acid on a microscope slide near the nozzle. The effect of adding acid vapor to the jet is shown in Figure 7. The cloudy jet in photo A has not been disturbed. Photo B shows that when

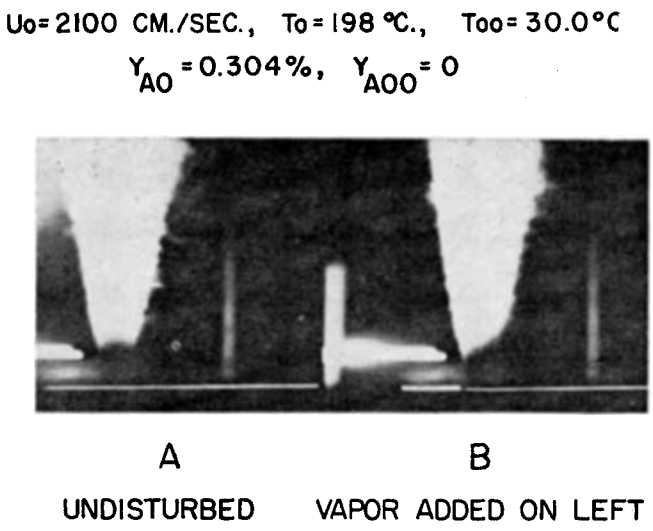

Fig. 7. Glycerine fog formation in jets, effect of addition of sulfuric acid vapor.

acid vapor enters the left side of the jet, fog forms nearer the nozzle. The traces of sulfuric acid vapor entrained in the jet with the fluid from the surroundings provided nuclei on which condensation took place. The nature of the nuclei is not known. A similar effect was noted by Higuchi and O'Konski (*12*).

The Mixing Zone and Fog Formation. These relatively simple visual observations demonstrated two important points: condensation is initiated in the mixing zone, and a supersaturated region probably exists in the mixing zone below the wedge of fog.

The importance of the mixing zone in the condensation process is not surprising, although it seems not to have been stressed before. This zone has long been of interest to workers in fluid mechanics. The streamlines of the mean flow are shown in Figure 8 taken from Prandtl (*21*, p. 123). Near the center of the jet the flow is parallel to the x axis. Along the outer edge of the jet the flow is directed radially inward before bending sharply upwards in the axial direction. The entrainment of cool air by the hot jet results in a sharp drop in temperature and concentration in the region between η_1 and η_2, which mark the edges of the mixing zone. There are thus two competing effects: cooling which tends to produce supersaturation, and dilution which tends to retard fog formation. If the initial concentration of vapor is sufficiently high, cooling produces condensation.

To shed further light on the mechanism of condensation detailed experimental measurements were made of the average values of the concentration $\overline{y}_A$, temperature $\overline{T}$, and velocity $\overline{U}$ in and near the mixing zone. The experimental methods are described in a previous section and in reference *11*. It was recognized that average values would not tell the whole story, since in the final step the condensation process occurs on a molecular scale. However the magnitude and extent of the zones of supersaturation could be calculated from $\overline{y}_A$ and $\overline{T}$. It was thought that useful information concerning the nature of the condensation process could be obtained from the distribution of supersaturation. Incidental to the main goal was the gathering of new experimental data on the characteristics

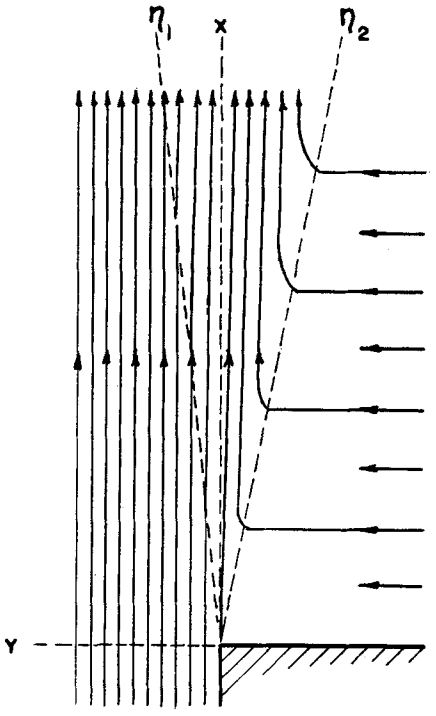

Fig. 8. Mean flow in the mixing zone.

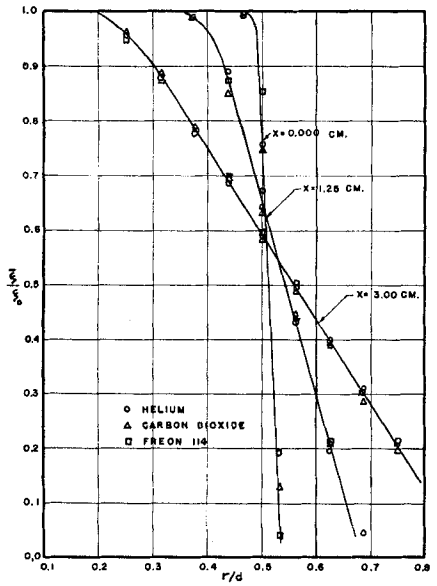

Fig. 9. Mean concentration in the mixing zone.

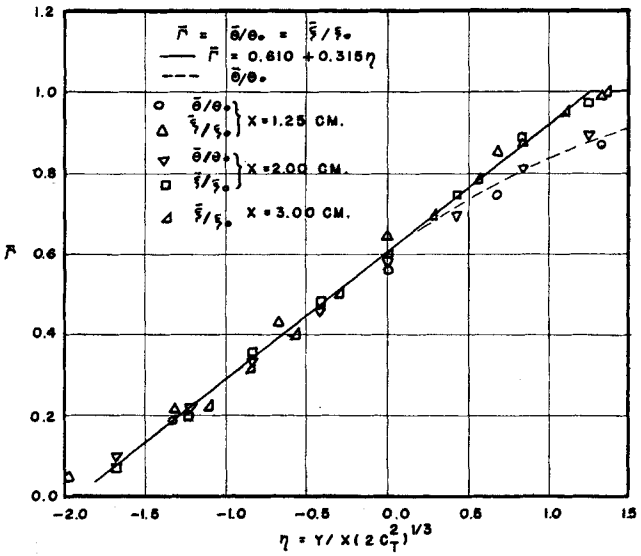

Fig. 11. Mean concentration and temperature in the mixing zone.

of the mixing zone, as well as some data for the transition zone and the fully developed region of flow.

Transport in the Mixing Zone

Distribution of Velocity, Temperature, and Concentration. The experimental results are shown in Table 2* and Figures 9 to 16. Figure 9 and Table 2B show the initial distributions of velocity and concentration of tracer gas. The profiles of velocity and concentration were nearly flat at $x = 0$ cm. The temperature distribution at $x = 0$ cm. could not be measured with the thermocouple probe. However the temperature profile at $x = 1.25$ cm. indicated that the initial temperature distribution was more rounded than the distributions of y_{Ao} and U_o, probably because of thermal losses at the nozzle edge. After $x/d \approx 3$, the dimensionless temperature and concentration distributions became nearly the same (Figures 12, 14, and 16). Matter and heat spread more rapidly than the x component of momentum.

The distributions of dimensionless concentration of helium ($y_{Ao} = 0.260\%$), carbon dioxide ($y_{Ao} = 0.850\%$), and freon-114 ($y_{Ao} = 0.350\%$) showed that these gases spread at the same rate even though their Schmidt numbers (ν/D_A) varied from 0.22 to 2.0 (Table 1). Examples of the radial profiles for the three tracer gases in the mixing zone are shown in Figure 9. The distributions of the three tracers coincided at succeeding sections downstream. The curves in Figures 12, 14, and 16 are based on the average concentrations of the three tracers. These observations extend and confirm the results of Hinze and Van der Hegge Zijnen (*14*) who reported similar behavior in the region of fully developed flow in an axially symmetric jet. They show that turbulent mixing and not molecular diffusion controls the spread of mean concentration in the mixing zone.

Near the nozzle the mean velocity profiles agreed fairly well with the boundary-layer analysis of Tollmien [Goldstein (*8*), p. 597] and Görtler [Schlichting (*23*), p. 598]. Figure 10 shows the variation of U/U_o with η for $x = 1.25$ to 4.00 cm. as compared with the theoretical curves. The initial conditions of the two theories require that the velocities at $x = 0$ be uniform. The rounded profile of U_o near the nozzle edge may account for the deviation of the data from the theoretical predictions.

Figure 11 shows that the dimensionless concentration profiles from $x = 0$ to 3 cm. varied linearly across the mixing zone as predicted by the vorticity transfer theory [Goldstein (*8*), p. 672]. The temperature profiles from $x = 0$ to 2 cm. are also included in Figure 11. These data

* Tabular material has been deposited as document 7763 with the American Documentation Institute, Photoduplication Service, Library of Congress, Washington 25, D. C., and may be obtained for $1.25 for photoprints or for 35-mm. microfilm.

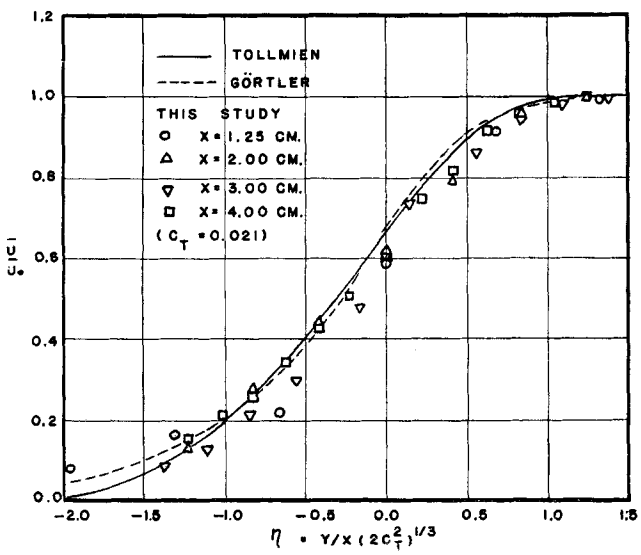

Fig. 10. Mean velocity profiles in the mixing zone.

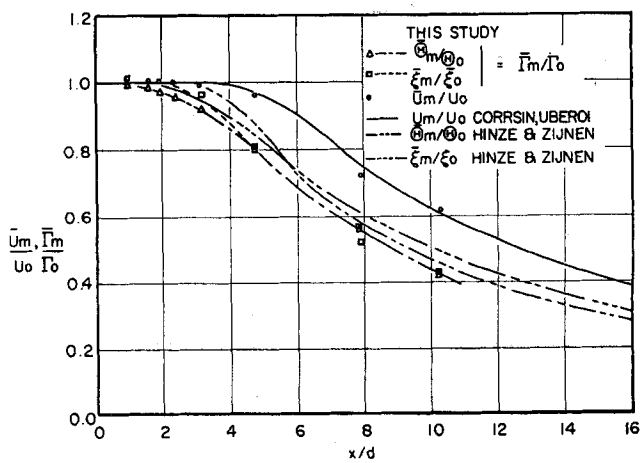

Fig. 12. Axial distribution of average properties in turbulent jet flow.

fall along the same line as the concentration data except near the inner boundary of the mixing zone ($\eta > 0.3$).

The following equation can be used to describe the concentration distribution in the mixing zone:

$$\bar{\xi} = 0.610 + 0.315\,\eta \qquad (2)$$

This equation correlates the temperature data of Corrsin (*4*) as well.

Downstream from the nozzle the axial distribution of mean properties follows the curves shown in Figure 12. The potential flow core disappeared at $x/d \approx 4$, while the zone of uniform temperature and concentration disappeared by $x/d \approx 2$. Although this value is somewhat less than that found by Corrsin and Uberoi (5), it compares favorably with the results of Hinze and Van der Hegge Zijnen (*14*). The radial distributions of mean velocity, temperature, and concentration in sections $x/d > 3$ are shown in Figures 13 to 16. In the transition region ($x/d \approx 4$ to 8) the profiles are not similar when plotted vs. $r/r_{1/2}$. ($r_{1/2}$ is the value of the radial co-ordinate where the dimensionless velocity is 0.5). The characteristic bell shaped distribution curves of the fully developed jet flow begin to appear at $x/d \approx 8$. In Figures 15 and 16 the distribution of dimensionless properties at $x/d = 10.2$ is compared with the data of other investigators for the fully developed region of flow. The mean velocity distribution is close to that of Corrsin and Uberoi (Figure 15). The distributions of concentration and temperature were similar to those of Corrsin and Uberoi but deviated somewhat from the data of Hinze and Van der Hegge Zijnen (Figure 16).

Mean and Fluctuating Supersaturations. The instantaneous local supersaturation in the turbulent jet is given by the conventional relation

$$S = \frac{y_A}{y_{AS}} \qquad (3)$$

The saturation concentration y_{AS} is a function only of the absolute temperature. Expanding y_{AS}^{-1} in a Taylor series around the local average temperature $\bar{T}$ one gets

$$S = y_A \left\{ \frac{1}{\bar{y}_{AS}} - \left(\frac{1}{y_{AS}^2} \frac{dy_{AS}}{dT} \right)_{T=\bar{T}} (T - \bar{T}) + \left[\frac{d^2(y_{AS}^{-1})}{dT^2} \right]_{T=\bar{T}} \frac{(T-\bar{T})^2}{2!} - \cdots \right\} \qquad (4)$$

In terms of the fluctuating temperature and concentration this becomes

$$S = \left(\frac{\bar{y}_A}{\bar{y}_{AS}} + \frac{y_A'}{\bar{y}_{AS}} \right) \left\{ 1 - \left(\frac{1}{y_{AS}} \frac{dy_{AS}}{dT} \right)_{T=\bar{T}} T' + \right.$$

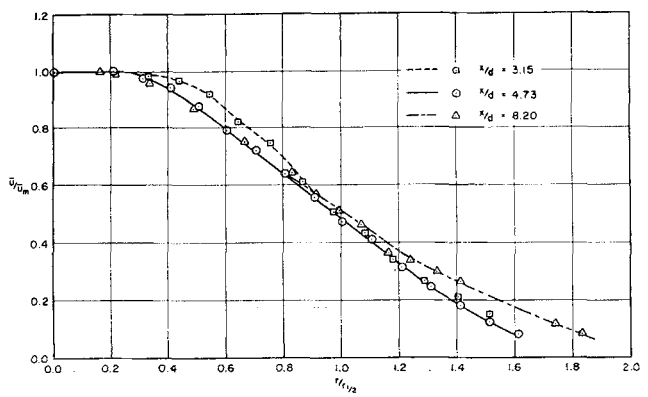

Fig. 13. Distribution of mean velocity in turbulent jet flow, x/d = 3.15 to 8.20.

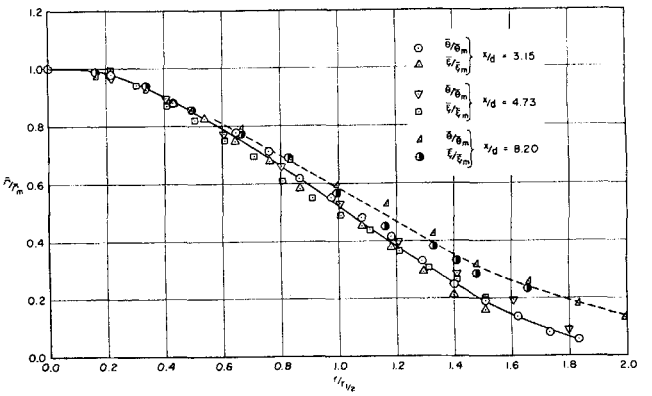

Fig. 14. Distribution of concentration and temperature in turbulent jet flow, x/d = 3.15 to 8.20.

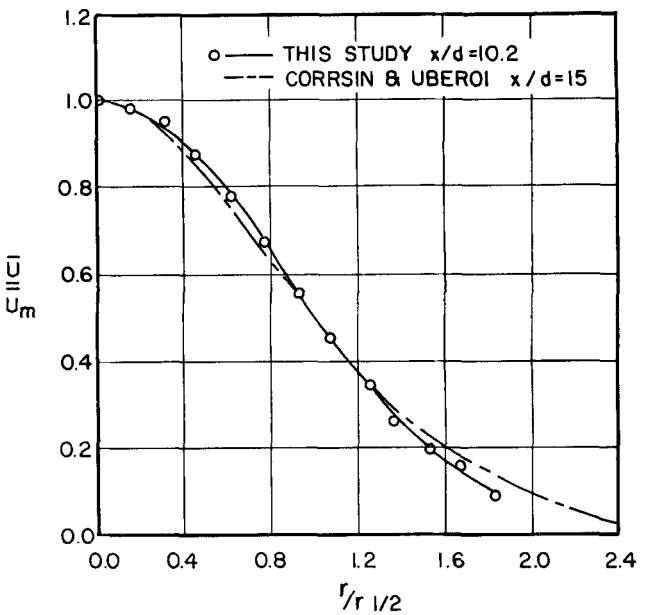

Fig. 15. Distribution of mean velocity in turbulent jet flow, $x/d > 10$.

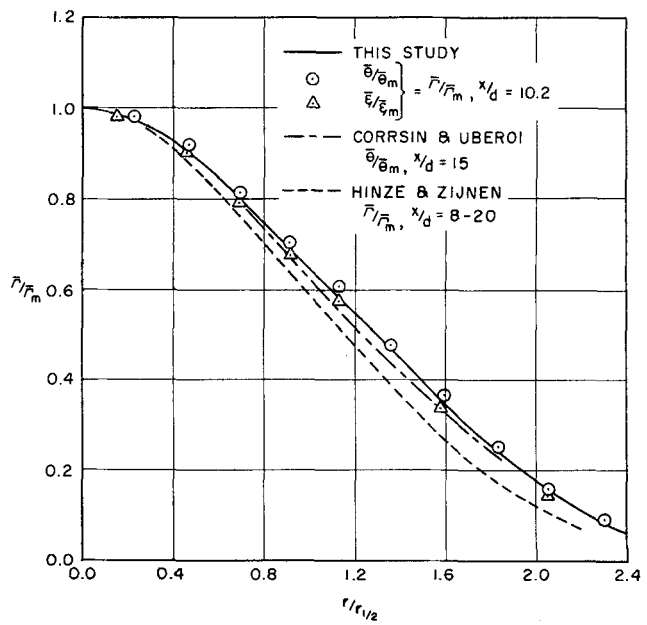

Fig. 16. Distribution of concentration and temperature in turbulent jet flow, $x/d > 10$.

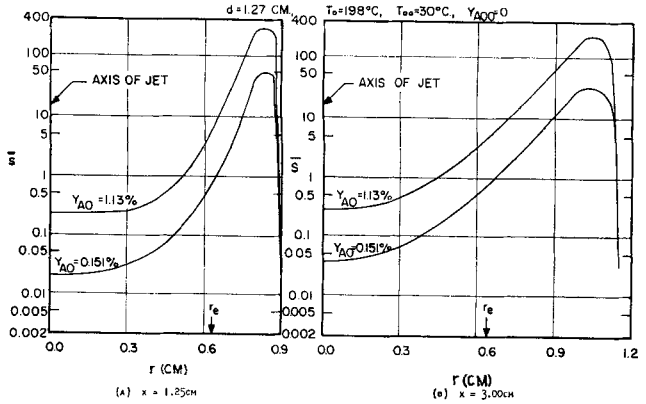

Fig. 17. Radial distribution of supersaturation, glycerine.

$$\bar{y}_{AS}\left[\frac{d^2(y_{AS}^{-1})}{dT^2}\right]_{T=\bar{T}}\frac{T'^2}{2!}-\cdots\Bigg\} \tag{5}$$

Neglecting the second-order and higher fluctuating quantities and using the Clausius-Clapeyron relation one obtains

$$S=\frac{\bar{y}_A}{\bar{y}_{AS}}+\frac{y_A'}{\bar{y}_{AS}}-\frac{\bar{y}_A\lambda T'}{\bar{y}_{AS}R\bar{T}^2} \tag{6}$$

The supersaturation may also be written in terms of local average and fluctuating quantities:

$$S=\bar{S}+s' \tag{7}$$

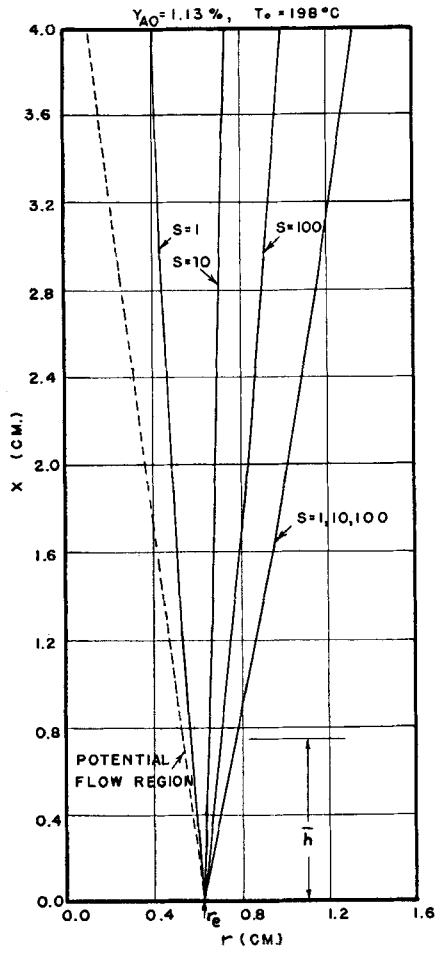

Fig. 18. Calculated contours of supersaturation, glycerine in air.

By comparison with the first-order approximation

$$\bar{S}=\frac{\bar{y}_A}{\bar{y}_{AS}} \tag{8}$$

$$s'=\frac{y_A'}{\bar{y}_{AS}}-\frac{\bar{S}\lambda T'}{R\bar{T}^2} \tag{9}$$

The average value of the fluctuating supersaturation vanishes as it should. It has two components, one resulting from the fluctuating concentration and the other from the fluctuating temperature. In the first-order approximation the average supersaturation is equal to the ratio of the average concentration to the average saturation concentration. This approximation will be best away from the central part of the mixing zone where the turbulent fluctuations are greatest, but it will be used throughout the discussion which follows.

Calculated Distribution of Supersaturation. From the measurements of the average temperature and concentration of noncondensable gas in the dry jet it was possible to calculate the distribution of supersaturation which would have existed in the absence of condensation. Figure 17 shows radial distribution curves of the supersaturation with respect to glycerine in the mixing zone for $x = 1.25$ and 3.00 cm. Very high supersaturations are reached near the outer edge of the mixing zone. Since $y_{A\infty} = 0$, a maximum value of S always occurs in the mixing zone.

From the concentration and temperature distributions it was also possible to determine surfaces of constant supersaturation. These are shown in cross section in Figure 18. There is a region of $\bar{S} < 1$ in the center of the jet and an inverted wedge shaped zone of $\bar{S} > 1$ extending tip downward to the nozzle edge. This geometry is also shown in the sketches of Figure 19. Figure 19A corresponds to a view of the jet seen in collimated light. The dotted line denotes the extent of the mixing zone, and the cross-hatched section represents the region of fog formation. The geometry of the round jet is shown in Figure 19B. The regions where $\bar{S}$ is equal to, greater, or less than unity are indicated along with the cross-hatched zone of fog formation.

Comparison of the zones of supersaturation with photographs (Figures 18 and 2B) indicated that fog was present in most of the region of $\bar{S} > 1$ except just upstream of $\bar{h}$, the tip of the wedge of fog. The fog filled region is cross hatched in Figure 19. A region of $\bar{S} >> 1$ existed upstream of $\bar{h}$ where no fog was observed. More detailed

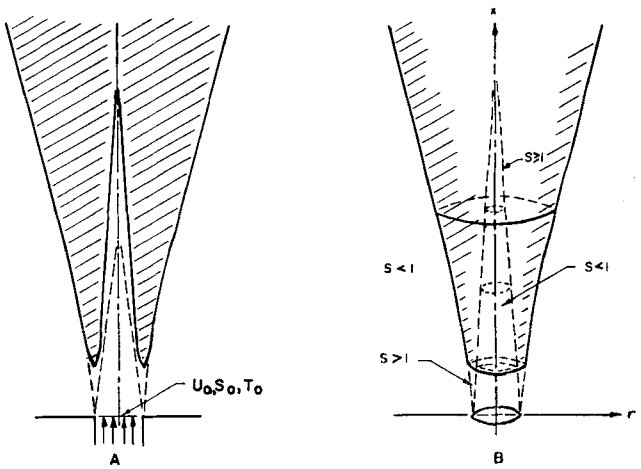

Fig. 19. Supersaturation and fog formation in a turbulent vapor jet.

calculations of the supersaturation along the inner edge of the condensation zone are given in a latter section.

Temperature Distribution in the Condensing Jet: The Condensation Front. Measurements were made of the temperature distribution in the jet carrying glycerine and dibutyl phthalate. The thermocouple was moved radially across the jet from the axis outward. At the point of entrance into the aerosol cloud moisture began to form on the joint between the iron and constantan wire (the thermocouple joint). At this location the measured temperature increased over the value found at the same point in the dry jet ($y_A = 0$). Figure 20 shows a typical curve of radial temperature measurements. Point A represents the location where the thermocouple entered the cloud and moisture formed on the thermocouple joint. When the probe was moved from the outer edge of the jet inwards, moisture formed on the thermocouple joint inside the outer boundary of the cloud. In Figure 20 point B represents the location where moisture formed on the wire, and point C is the outer extent of the visible cloud. The temperature difference between the wet and dry jet profiles extends over the mixing zone between the points A and B. This zone indicates the region where appreciable condensation occurs. Along the outer boundary droplets of fog were carried away from the region of condensation by the turbulent eddies.

When the initial concentration was decreased, the magnitude of the temperature rise also decreased until the dry jet profile was approached as shown in Figure 21. This drawing is an enlargement of the region of radial temperature distributions of interest at $x = 3.00$ cm. The condensation zone became less well-defined visually as the initial concentration decreased. The region where fog was visible became narrower as can be seen by comparing Figures 2B and 2D. Similarly the locations where moisture formed on the thermocouple joint moved closer together with decreasing concentration. In Figure 21 points A, B ($y_{Ao} = 1.13\%$), points C, D ($y_{Ao} = 0.659\%$) and points E, F ($y_{Ao} = 0.151\%$) denote the limits of condensation defined by the onset of moisture on the thermocouple joint.

It is easy to interpret the temperature rise measured by the thermocouple if thermodynamic equilibrium exists in the condensation zone. At equilibrium the gas phase is saturated, and the temperatures of the gas and the liquid droplets are equal. The local wet and dry bulb temperatures are the same, and this is the temperature measured by the wetted thermocouple. The temperature rise in the condensation zone results from the release of latent heat during fog formation.

The measurements of temperature increase in the condensation zone are new. These data and the visual observations indicate that fog forms along a well-defined

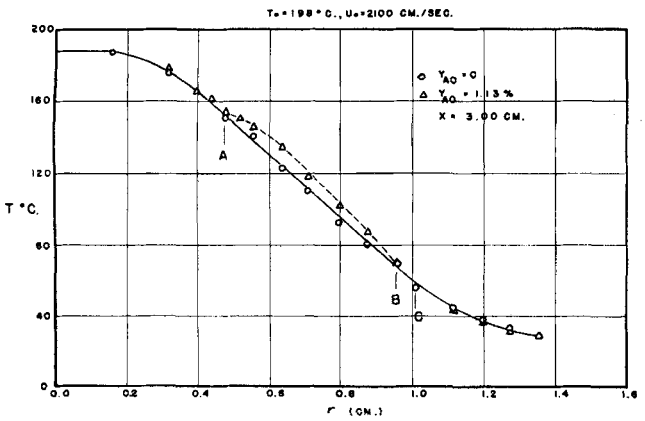

Fig. 20. Temperature increase across the condensation zone, glycerine in air.

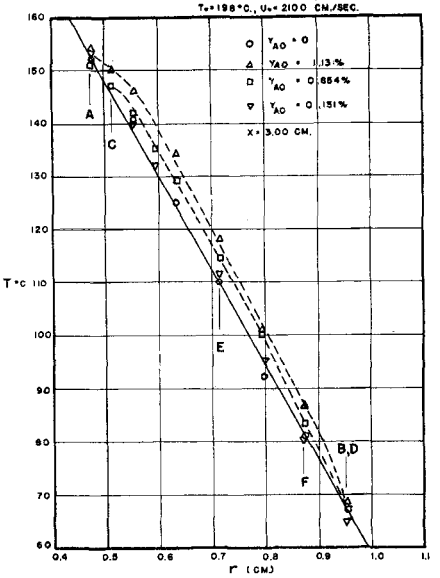

Fig. 21. Temperature increase in the condensation zone, glycerine.

surface at the inner boundary of the mixing zone. This surface does not coincide with the edge of the potential core but lies somewhat downstream. The region of transition will be designated the *condensation front.* The condensation front in the mixing zone appeared over a wide range of initial vapor concentration. This phenomenon has certain similarities to the condensation shock which may occur in the diverging section of supersonic nozzles (*26, 30*). The condensation front (shock) associated with supersonic flow is characterized by a sudden onset of visible fog and an increase in static pressure at the point of fog formation. The increase in pressure is attributed to the release of latent heat during condensation.

Supersaturation at the Condensation Front. Calculations of $\overline{S}$ for glycerine and dibutyl phthalate fogs were made from the concentration profiles and the dry jet temperature at the point where moisture began to form on the thermocouple joint. The values of y_{As} were obtained from data of Stedman (*25*) for glycerine and from Small, Small, and Cowley (*24*) for dibutyl phthalate. The calculated values of the supersaturation at the inner boundary of the condensation zone are tabulated in Table 3. The probable error arising from the experimental technique, excluding the effect of turbulence and error in vapor pressure data, is shown with the values of $\overline{S}$ in Table 3. The details of the calculation of the probable error are given in reference *11.*

The data in Table 3 show that the values of $\overline{S}$ at the condensation front were about the same regardless of the traversing position x. The values remained approximately constant and near unity over a range of glycerine concentration from $y_{Ao} = 1.13$ to 0.151%. The values calculated for dibutyl phthalate were also approximately constant but somewhat higher than those found for glycerine. The calculation gave self-consistent and reproducible values for the supersaturation along the inner boundary of the condensation zone for each material.

The deviation of the calculated values of $\overline{S}$ from unity and the difference in S between glycerine and dibutyl phthalate may result from errors in the vapor pressure data. The data of Stedman (*25*) for glycerine agree with data of Trevoy (*28*) and Filosofo et al. (*6*). They do not agree with the results of Zil'berman-Granovskaya (*19*). The data of Small, Small, and Cowley (*24*) for dibutyl

TABLE 3. CALCULATED SUPERSATURATION AT THE INNER BOUNDARY OF THE CONDENSATION ZONE

A. Glycerine (U_o = 2,100 cm./sec., T_o = 198°C., T_{oo} = 30.0°C.)

	y_{Ao}(%)	x(cm.)	$\overline{T}$(°K.)	$\overline{S}$
1.	1.13	1.25	427	1.39 ± 0.16
		2.00	428	1.26 ± 0.16
		3.00	427	1.25 ± 0.19
2.	0.659	1.25	415	1.46 ± 0.17
		2.00	419	1.12 ± 0.18
		3.00	414	1.32 ± 0.15
3.	0.151	1.25	384	1.51 ± 0.23
		2.00	382	1.37 ± 0.24
		3.00	385	1.32 ± 0.22

B. Dibutyl phthalate (U_o = 2,190 cm./sec., T_o = 226°C., T_{oo} = 30.0°C.)

	y_{Ao}(%)	x(cm.)	$\overline{T}$(°K.)	$\overline{S}$
1.	0.183	2.00	398	2.96 ± 0.46
		3.00	401	2.35 ± 0.32
2.	0.185	2.00	399	2.74 ± 0.40
		3.00	401	2.35 ± 0.32

phthalate agree with those of Hickman (*10*) over the range of 50° to 100°C.

Mechanism of Condensation

Condensation on Atmospheric Nuclei. The rate at which condensation occurs from the supersaturated vapor on one of the particles of the atmospheric aerosol can be estimated from the relationship for the flux to a spherical sink in an infinite stagnant medium:

$$J = 4\pi a D_A (n - n_s) \tag{10}$$

The fractional rate of change of the glycerine vapor concentration resulting from condensation on the atmospheric aerosol is given by

$$\frac{1}{n}\frac{dn}{dt} = 4\pi a D_A \left(1 - \frac{1}{S}\right) n_p \tag{11}$$

The fractional rate of change of concentration resulting from condensation on the atmospheric particles would be a maximum were S equal to infinity. In this case

$$\left(\frac{1}{n}\frac{dn}{dt}\right)_{\max} = 4\pi a D_A n_p$$

Based on experiments carried out by Pasceri (*20*) reasonable values for n_p and a in Baltimore are 10^4 particles/cc. and 10^{-5} cm., respectively. The diffusion coefficient of the vapor molecules can be taken to be 10^{-1} sq. cm./sec. Substituting one gets

$$\left(\frac{1}{n}\frac{dn}{dt}\right)_{\max} \approx 4\pi (10)^{-1} (10)^{-5} (10)^{4}$$
$$\approx 10^{-1}\ \text{sec}^{-1}$$

That is the concentration of glycerine vapor would decrease at a rate of 0.1 of the total amount present per second if the supersaturation were infinite or, for all practical purposes, greater than 10. The approximate time necessary for the vapor leaving the nozzle to reach the zone where condensate becomes visible in these experiments is given by

$$\tau \approx \frac{\overline{h}}{U_o}$$
$$\approx 10^{-3}\ \text{sec}$$

Hence in the time necessary to reach the condensation zone, 10^{-1} $(10)^{-3}$ or only one ten thousand of the total vapor present could have condensed on the atmospheric aerosol under the most favorable circumstances. It would take a particle concentration 10^2 or 10^3 higher than actually present to contribute significantly to condensation in the time available.

Proposed Mechanism. Calculations based on the measurements of temperature and concentration indicate that high values of the supersaturation are reached at the beginning of the mixing zone upstream of the wedge of fog. This conclusion is consistent with observations of the effects of inserting wires and adding nuclei to the mixing zone. The calculations of the last section indicate that the concentration of the atmospheric aerosol is not sufficient to relieve the supersaturation resulting in a rapid mixing process. Hence it is concluded that homogeneous nucleation in the highly supersaturated regions near the nozzle initiates fog formation. An attempt was made to estimate the fractional rate of change of concentration by homogeneous nucleation with the Becker-Döring theory. The uncertainties in the calculations were considered too serious to justify its presentation.

Downstream from the point where condensation first began the fog filled most of that region of the mixing zone where the average supersaturation was greater than unity. This result can be explained by the effect of turbulent mixing. After homogeneous nucleation in regions of $S >> 1$, fog is carried by the turbulent eddies into zones of $S \approx 1$, just as a stable smoke introduced at a point near the nozzle is dispersed through the mixing zone. The location of the fog as determined in these experiments was based on time averaged temperature and optical density; for at least part of the time supersaturated vapor must have been present in the region $\overline{S} \approx 1$. In the turbulent exchange process supersaturated vapor from the inner edge of the cloud is carried into the mixing zone and probably seeded by embryos produced by homogeneous nucleation. In effect these embryos serve as foreign nuclei.

The effects of turbulent mixing followed by molecular diffusion of vapor and embryos make the jet method seem unpromising for quantitative tests of theories of condensation such as that of Becker-Döring. Analyses that attempt to relate gross scale measurements of particle concentration to an integral average generation rate over the surfaces of constant average supersaturation may be in error. If nuclei are formed by homogeneous nucleation primarily in regions near the nozzle, integration over a volume of the jet where S is greater than 1 should predict excessively high values of the average rate of particle production. Hence there may be some doubt concerning the interpretation of the results of Higuchi and O'Konski (*12*).

SUMMARY AND CONCLUSIONS

1. Condensation occurred in the mixing zone of the jet.
2. The cross section of the condensation zone appeared as a wedge with its tip located near the mouth of the nozzle. The wedge of fog surrounded a conical region where vapor remained unsaturated.
3. The onset of visible fog formation in the mixing zone depended on the state of the fluid at the nozzle and the surrounding medium.
4. After $x/d \approx 3$, measured concentration and temperature profiles presented in dimensionless form were nearly the same up to x/d = 10.2. The difference between the profiles near the nozzle is attributed to the inequality of the initial conditions of temperature and concentration of tracer gas.
5. Momentum diffused less rapidly than heat and matter in the turbulent jet.

6. Gases ranging in Schmidt number based on molecular properties from 0.22 to 2.0 dispersed at the same average rate in the jet.

7. Measured fields of mean velocity, temperature, and concentration of tracer gas in the mixing zone were correlated with predictions from the theory of turbulent boundary layers. The data of this study compared favorably with existing experimental results in the region of fully developed turbulent jet flow.

8. Calculated zones of supersaturation showed that visible fog was present in the regions $x > \bar{h}$ near $\bar{S} = 1$.

9. A measurable temperature effect was associated with the onset of fog.

10. Evidence was found that homogeneous nucleation controlled the initial stages of fog formation in spite of the presence of the normal atmospheric aerosol. Molecular clusters generated in regions of $\bar{S} >> 1$ near the nozzle edge acted as nuclei for condensation further downstream in the mixing zone where $S \approx 1$.

ACKNOWLEDGMENT

The authors wish to express their appreciation for the support accorded G. M. Hidy by the Shell Companies Foundation and the National Center for Atmospheric Research during part of the period of this study. This work was supported in part by Atomic Energy Commission Contract AT(30-1)-2165.

NOTATION

a = radius of aerosol particle, cm.
c_T = constant of proportionality in analysis of mixing zone ($c_T = 0.021$)
C_p = specific heat, cal./g.
d = diameter of nozzle, cm.
D_A = diffusivity of vapor or tracer gas, sq. cm./sec.
h = distance from the nozzle to the aerosol cloud, cm.
J = molar flux of vapor, moles/sec.
k = thermal conductivity, cal./sq. cm. sec. (°C./cm.)
L = characteristic length
n = molar concentration of vapor, moles/cc.
n_s = concentration of vapor at the surface of the aerosol particle, moles/cc.
n_p = concentration of particles of radius a in the atmosphere, cc.$^{-1}$
N_{Le} = Lewis number ($\rho D_A C_p/k$)
N_{Pr} = Prandtl number ($C_p \rho \nu/k$)
N_{Sc} = Schmidt number (ν/D_A)
r = radial coordinate
r_e = value of r at the edge of the nozzle, cm.
$r_{1/2}$ = value of r where $\bar{U}$ is one-half $\bar{U}_m$, cm.
R = gas constant
S = supersaturation (y_A/y_{AS})
T = temperature, °C. or °K.
U = axial component of velocity, cm./sec.
V = characteristic velocity
x = axial coordinate
y = lateral coordinate in the two-dimensional model of the mixing zone ($r_e - r$)
y_A = mole fraction of vapor or tracer gas in air

Greek Letters

Γ = dimensionless concentration or temperature (ξ or θ)
η = dimensionless coordinate ($y/x(2c_T^2)^{1/3}$
η_1, η_2 = values of η at the edges of the mixing zone
θ = dimensionless temperature ($T - T_\infty/T_o - T_\infty$)
λ = latent heat of vaporization, cal./mole
ν = kinematic viscosity, sq. cm./sec.
ξ = dimensionless concentration ($y_A - y_{A\infty}/y_{Ao} - y_{A\infty}$)
ρ = mass density, g./cc.
τ = characteristic time ($\bar{h}/\bar{U}_o$), sec.
τ_c = mean time between molecular collisions among molecules of condensing vapor, sec.

Subscripts

m = maximum value of a property at x
o = value of property at the nozzle
∞ = value of property at ambient conditions
s = value of property at saturation conditions

The bar (—) above a quantity indicates that it is averaged with respect to time, while the prime (′) indicates a fluctuating value.

LITERATURE CITED

1. Amelin, A. G., *Kolloid. Zhur.*, **10**, 168 (1948).
2. ———, and M. I. Belakov, *ibid.*, **17**, 10 (1955).
3. Appleman, H., *Bull. Am. Met. Soc.*, **34**, 14 (1953).
4. Corrsin, S., *NACA Wartime Rept. ACR 3L23* (1943).
5. ———, and M. Uberoi, *NACA Rept.* 998 (1950).
6. Filosofo, I., M. Merlin, and A. Rostagni, *Nuovo Cimento*, **7**, 69 (1956).
7. Friedlander, S. K., *Phys. Fluids*, **3**, 693 (1960).
8. Goldstein, S., "Modern Developments in Fluid Dynamics," Vol. 2, Oxford University Press, England (1938).
9. Green, H. L., and W. R. Lane, "Particulate Clouds: Dusts, Smokes and Mists," E. and F. N. Spon, London, England (1957).
10. Hickman, K. C. D., J. C. Hecker, and N. D. Embree, *Ind. Eng. Chem., (Anal. Ed.)*, **9**, 264 (1937).
11. Hidy, G. M., D.Eng. thesis, Johns Hopkins University, Baltimore, Maryland (1962).
12. Higuchi, W. I., and C. T. O'Konski, *J. Colloid Sci.*, **15**, 14 (1960).
13. Hinze, J. O., "Turbulence," McGraw-Hill, New York (1959).
14. ———, and B. G. Van der Hegge Zijnen, *Appl. Sci. Res.*, **A1**, 435 (1949).
15. Johnstone, H. F., and D. K. Eads, *Ind. Eng. Chem.*, **42**, 2293 (1950).
16. Levine, D., and S. K. Friedlander, *Chem. Eng. Sci.*, **13**, 49 (1960).
17. May, D., and D. Decker, "Diffusion of Glycerine Vapor in Air," Unpubl. Lab. Report, Chem. Eng. Dept., Johns Hopkins University, Baltimore, Maryland (1960).
18. McAdams, W. H., "Heat Transmission," 3 ed., McGraw-Hill, New York (1954).
19. Miner, C. S., and N. N. Dalton, ed., "Glycerol," Reinhold, New York (1953).
20. Pasceri, R. E., Unpubl. Report, Chem. Eng. Dept., Johns Hopkins University, Baltimore, Maryland (1962).
21. Prandtl, L., "Essentials of Fluid Dynamics," Blackie and Son, London, England (1948).
22. Reid, R. C., and T. K. Sherwood, "The Properties of Gases and Liquids," Ch. 8, McGraw-Hill, New York (1958).
23. Schlichting, H., "Boundary Layer Theory," 4 ed., McGraw-Hill, New York (1960).
24. Small, P. A., K. W. Small, and P. Cowley, *Trans. Faraday Soc.*, **44**, 810 (1948).
25. Stedman, D. F., *ibid.*, **24**, 296 (1938).
26. Stever, H. G., in "Fundamentals of Gas Dynamics," Emmons, H. W., ed., Princeton Univ. Press, Princeton, New Jersey (1956).
27. Townsend, A. A., "The Structure of Turbulent Shear Flow," Ch. 8, Cambridge Univ. Press, England (1956).
28. Trevoy, D. J., *Ind. Eng. Chem.*, **45**, 2366 (1953).
29. Washburn, E. W., ed., "International Critical Tables, Vol. 5, McGraw-Hill, New York (1937).
30. Wegner, P. P., and L. M. Mack, in "Advances in Applied Mechanics," Vol. 5, Academic Press, New York (1958.)

Manuscript received March 29, 1963; revision received July 10, 1963; paper accepted July 12, 1963. Paper presented at A.I.Ch.E. San Juan meeting.